

Manipulating spin-dependent splitting of vector abruptly autofocusing beam by encoding cosine-azimuthal variant phases

YI ZHANG,¹ PENG LI,^{1,2} SHENG LIU,¹ LEI HAN,¹ HUACHAO CHENG,¹ AND JIANLIN ZHAO^{1,3}

¹Key Laboratory of Space Applied Physics and Chemistry, Ministry of Education, and Shaanxi Key Laboratory of Optical Information Technology, School of Science, Northwestern Polytechnical University, Xi'an 710072, China

²pengli@nwpu.edu.cn

³jlzhao@nwpu.edu.cn

Abstract: We report the realization of spin-dependent splitting of vector abruptly autofocusing beam (AAB) by encoding cosine-azimuthal variant phases. By employing the local spatial frequency (LSF), we reveal an approximation mapping relationship between focal field intensity of the two spin components and the pertinent phase distribution of input field. As well as theoretical analysis, we present experimental demonstrations of this guidance. Special focal field intensity, polarization and phase are realized by consciously managing the cosine-azimuthal variant phase. This distinctive focal field of vector AAB may have a broad range of applications in harnessing the spin-orbit coupling, optical trapping and laser machining.

© 2016 Optical Society of America

OCIS codes: (050.1940) Diffraction; (260.5430) Polarization; (140.3300) Laser beam shaping; (050.4865) Optical vortices.

References and links

1. J. T. Hunt, P. A. Renard, and R. G. Nelson, "Focusing properties of an aberrated laser beam," *Appl. Opt.* **15**(6), 1458–1464 (1976).
2. K. Youngworth and T. Brown, "Focusing of high numerical aperture cylindrical-vector beams," *Opt. Express* **7**(2), 77–87 (2000).
3. Q. Zhan and J. Leger, "Focus shaping using cylindrical vector beams," *Opt. Express* **10**(7), 324–331 (2002).
4. K. Y. Bliokh, E. A. Ostrovskaya, M. A. Alonso, O. G. Rodriguez-Herrera, D. Lara, and C. Dainty, "Spin-to-orbital angular momentum conversion in focusing, scattering, and imaging systems," *Opt. Express* **19**(27), 26132–26149 (2011).
5. Z. Chen, T. Zeng, and J. Ding, "Reverse engineering approach to focus shaping," *Opt. Lett.* **41**(9), 1929–1932 (2016).
6. N. K. Efremidis and D. N. Christodoulides, "Abruptly autofocusing waves," *Opt. Lett.* **35**(23), 4045–4047 (2010).
7. D. G. Papazoglou, N. K. Efremidis, D. N. Christodoulides, and S. Tzortzakis, "Observation of abruptly autofocusing waves," *Opt. Lett.* **36**(10), 1842–1844 (2011).
8. P. Zhang, J. Prakash, Z. Zhang, M. S. Mills, N. K. Efremidis, D. N. Christodoulides, and Z. Chen, "Trapping and guiding microparticles with morphing autofocusing Airy beams," *Opt. Lett.* **36**(15), 2883–2885 (2011).
9. A. Chong, W. H. Renninger, D. N. Christodoulides, and F. W. Wise, "Airy-Bessel wave packets as versatile linear light bullets," *Nat. Photonics* **4**(2), 103–106 (2010).
10. P. Panagiotopoulos, D. G. Papazoglou, A. Couairon, and S. Tzortzakis, "Sharply autofocused ring-Airy beams transforming into non-linear intense light bullets," *Nat. Commun.* **4**, 2622 (2013).
11. S. Liu, M. Wang, P. Li, P. Zhang, and J. Zhao, "Abrupt polarization transition of vector autofocusing Airy beams," *Opt. Lett.* **38**(14), 2416–2418 (2013).
12. G. A. Siviloglou, J. Broky, A. Dogariu, and D. N. Christodoulides, "Observation of accelerating Airy beams," *Phys. Rev. Lett.* **99**(21), 213901 (2007).
13. I. Chremmos, P. Zhang, J. Prakash, N. K. Efremidis, D. N. Christodoulides, and Z. Chen, "Fourier-space generation of abruptly autofocusing beams and optical bottle beams," *Opt. Lett.* **36**(18), 3675–3677 (2011).
14. I. Chremmos, N. K. Efremidis, and D. N. Christodoulides, "Pre-engineered abruptly autofocusing beams," *Opt. Lett.* **36**(10), 1890–1892 (2011).
15. J. A. Davis, D. M. Cottrell, and D. Sand, "Abruptly autofocusing vortex beams," *Opt. Express* **20**(12), 13302–13310 (2012).

16. Y. Jiang, K. Huang, and X. Lu, "Propagation dynamics of abruptly autofocusing Airy beams with optical vortices," *Opt. Express* **20**(17), 18579–18584 (2012).
17. B. Chen, C. Chen, X. Peng, Y. Peng, M. Zhou, and D. Deng, "Propagation of sharply autofocused ring Airy Gaussian vortex beams," *Opt. Express* **23**(15), 19288–19298 (2015).
18. P. Li, S. Liu, T. Peng, G. Xie, X. Gan, and J. Zhao, "Spiral autofocusing Airy beams carrying power-exponent-phase vortices," *Opt. Express* **22**(7), 7598–7606 (2014).
19. Q. Zhan, "Cylindrical vector beams: from mathematical concepts to applications," *Adv. Opt. Photonics* **1**(1), 1–57 (2009).
20. H. Wang, L. Shi, B. Lukyanchuk, C. Sheppard, and C. T. Chong, "Creation of a needle of longitudinally polarized light in vacuum using binary optics," *Nat. Photonics* **2**(8), 501–505 (2008).
21. H. Lin, B. Jia, and M. Gu, "Generation of an axially super-resolved quasi-spherical focal spot using an amplitude-modulated radially polarized beam," *Opt. Lett.* **36**(13), 2471–2473 (2011).
22. X. Gao, D. Zhang, T. Mei, R. Fu, and S. Zhuang, "Focus shaping of the radially polarized Bessel–Gauss beam with a sine-azimuthal variation wavefront," *Opt. Appl.* **43**(3), 567–582 (2013).
23. X. Jiao, S. Liu, Q. Wang, X. Gan, P. Li, and J. Zhao, "Redistributing energy flow and polarization of a focused azimuthally polarized beam with rotationally symmetric sector-shaped obstacles," *Opt. Lett.* **37**(6), 1041–1043 (2012).
24. W. Zhang, S. Liu, P. Li, X. Jiao, and J. Zhao, "Controlling the polarization singularities of the focused azimuthally polarized beams," *Opt. Express* **21**(1), 974–983 (2013).
25. P. Li, S. Liu, G. Xie, T. Peng, and J. Zhao, "Modulation mechanism of multi-azimuthal masks on the redistributions of focused azimuthally polarized beams," *Opt. Express* **23**(6), 7131–7139 (2015).
26. P. Li, S. Liu, Y. Zhang, G. Xie, and J. Zhao, "Experimental realization of focal field engineering of the azimuthally polarized beams modulated by multi-azimuthal masks," *J. Opt. Soc. Am. B* **32**(9), 1867–1872 (2015).
27. X. Xie, Y. Chen, K. Yang, and J. Zhou, "Harnessing the point-spread function for high-resolution far-field optical microscopy," *Phys. Rev. Lett.* **113**(26), 263901 (2014).
28. X. L. Wang, J. Chen, Y. Li, J. Ding, C. S. Guo, and H. T. Wang, "Optical orbital angular momentum from the curl of polarization," *Phys. Rev. Lett.* **105**(25), 253602 (2010).
29. M. Neugebauer, T. Bauer, P. Banzer, and G. Leuchs, "Polarization tailored light driven directional optical nanobeacon," *Nano Lett.* **14**(5), 2546–2551 (2014).
30. V. D'Ambrosio, N. Spagnolo, L. Del Re, S. Slussarenko, Y. Li, L. C. Kwek, L. Marrucci, S. P. Walborn, L. Aolita, and F. Sciarrino, "Photonic polarization gears for ultra-sensitive angular measurements," *Nat. Commun.* **4**, 2432 (2013).
31. C. Gabriel, A. Aiello, W. Zhong, T. G. Euser, N. Y. Joly, P. Banzer, M. Förtsch, D. Elser, U. L. Andersen, Ch. Marquardt, P. St. J. Russell, and G. Leuchs, "Entangling different degrees of freedom by quadrature squeezing cylindrically polarized modes," *Phys. Rev. Lett.* **106**(6), 060502 (2011).
32. G. Milione, T. A. Nguyen, J. Leach, D. A. Nolan, and R. R. Alfano, "Using the nonseparability of vector beams to encode information for optical communication," *Opt. Lett.* **40**(21), 4887–4890 (2015).
33. S. B. Wang and C. T. Chan, "Lateral optical force on chiral particles near a surface," *Nat. Commun.* **5**, 3307 (2014).
34. K. Y. Bliokh, F. J. Rodriguez-Fortuno, F. Nori, and A. V. Zayats, "Spin-orbit interactions of light," *Nat. Photonics* **9**(12), 796–808 (2015).
35. J. E. Curtis and D. G. Grier, "Modulated optical vortices," *Opt. Lett.* **28**(11), 872–874 (2003).
36. Y. Zhang, P. Li, S. Liu, and J. Zhao, "Unveiling the photonic spin Hall effect of freely propagating fan-shaped cylindrical vector vortex beams," *Opt. Lett.* **40**(19), 4444–4447 (2015).
37. C. Alonzo, P. J. Rodrigo, and J. Glückstad, "Helico-conical optical beams: a product of helical and conical phase fronts," *Opt. Express* **13**(5), 1749–1760 (2005).
38. O. Bryngdahl, "Geometrical transformations in optics," *J. Opt. Soc. Am.* **64**(8), 1092–1099 (1974).
39. M. Born and E. Wolf, *Principles of Optics*, 7th ed. (Cambridge University, 1999).
40. D. Zhang, X. Feng, K. Cui, F. Liu, and Y. Huang, "Identifying Orbital Angular Momentum of Vectorial Vortices with Pancharatnam Phase and Stokes Parameters," *Sci. Rep.* **5**, 11982 (2015).

1. Introduction

The focusing properties of light fields, as one of the most important aspect of light propagation, have always been playing an important role in the practical applications of optics. In the past decades, the focusing engineering of light fields has been investigated extensively in various realms [1–5]. Recently, the abruptly autofocusing beam (AAB) has emerged as an unusual approach to deliver drastically enhanced intensity with small spot size on a remote target. Such an interesting AAB was firstly proposed theoretically by Efremidis *et al.* [6] and demonstrated experimentally by Papazoglou *et al.* [7]. The abrupt intensity increase without any lens or nonlinearity makes the AAB an ideal candidate to deliver high

energy without damaging the material before the focus, which has a variety of applications in guiding micro-particles [8], light bullets [9,10] and spin-orbit coupling [11].

Ring Airy beams, i.e., the beams with circularly symmetric Airy radial amplitude, are the first AAB to be studied, which can produce fascinating behaviors such as parabolic trajectory, diffraction-resisting and transverse acceleration [12–14]. The manipulation on the autofocusing property of ring Airy beams by modulating the initial phase distribution has been theoretically and experimentally demonstrated. For instance, the focal distance and size of the focus spot are adjustable via attaching vortex phases [15–17], and spiral autofocus occurs via encoding a power-exponent-phase vortex phase [18]. Besides the scalar fields, steering the abruptly autofocusing property of ring Airy beam based on the modulation of polarization has also attracted rapidly growing interests [11]. It is well known that, the focusing properties of vector fields with inhomogeneous polarization distributions have been extensively investigated [19–26], and demonstrated that they are of interest for applications in high resolution optical microscopy [27], optical manipulation [28,29], angular measurement [30], quantum information [31] and optical communication [32]. The AAB possessing inhomogeneous polarization distributions has exhibited interesting spin-orbital angular momenta interaction and polarization singularities conversion [11]. Hence, as we can see, by simultaneously modulating initial phase and polarization distributions of AABs, it is possible to produce high energy focal field with special spin angular momentum (SAM) and orbital angular momentum (OAM) distributions, which may be used in applications including optical detection of chiral particles [33], spin-orbital optical interaction [11,34], reconfigurable dynamical intensity optical trap [35], laser medical treatment and laser machining [6,7]. However, the joint effect of polarization and phase distribution on the focal field of AAB is still scarce.

In this paper, we simultaneously employ cosine-azimuthal variant phase and second order vector polarization distributions to steer the spin-dependent splitting of AAB in the focal field. The vector AAB with cosine-azimuthal variant phase can be decomposed into two spin components, i.e., left- (LH) and right-handed (RH) circular polarizations, with diverse initial phase. Based on the local spatial frequency (LSF) of the two spin components, an approximation mapping relationship between focal field intensity and initial phase of the two spin components is predicted. Furthermore, by setting the cosine-azimuthal variant phase parameter, the spin-dependent splitting and carried OAM in the focal field can be controlled.

2. Theory analysis

For a cylindrically polarized AAB with cosine-azimuthal variant phase, the complex vector field can be described as

$$\mathbf{E}(r, \varphi) = E_0(r) [\cos(m\varphi + \varphi_0) \mathbf{x} + \sin(m\varphi + \varphi_0) \mathbf{y}] \exp(i \cos n\varphi). \quad (1)$$

where $E_0(r) = \text{Ai}[(r_0-r)/\omega] \exp[\alpha(r_0-r)/\omega]$, $\text{Ai}(\cdot)$ denotes the Airy function, r is the radius, r_0 is the radius of primary ring, ω is a scaling factor and α is the exponential decay factor; m is the polarization order of cylindrical vector beam; φ is the azimuthal coordinate; φ_0 is the initial polarization direction for $\varphi = 0$; n is the cosine-azimuthal variant phase parameter; \mathbf{x} and \mathbf{y} are the unit vector along the x and y axes, respectively. To analyze the focal field properties of the vector AAB, we resort to its Fraunhofer diffraction field. For simplicity, we firstly decompose such a light field into two spin components. Hence, the field expressed by Eq. (1) can also be denoted as

$$\mathbf{E}(r, \varphi) = E_0(r) \left\{ \exp[-i(m\varphi + \varphi_0 - \cos n\varphi)] \mathbf{L} + \exp[i(m\varphi + \varphi_0 + \cos n\varphi)] \mathbf{R} \right\} / \sqrt{2}, \quad (2)$$

where \mathbf{L} and \mathbf{R} denote the unit vectors of LH and RH circular polarizations, respectively. Thereby, the far-field envelope of the vector AAB can be described by Fresnel integration in cylindrical coordinates as [25,36]

$$U(\rho, \phi, z) = \frac{1}{i2\sqrt{2\pi}\lambda z} \exp\left(\frac{ik\rho^2}{2z}\right) \iint E_0(r) \left\{ \exp[-i(m\varphi + \varphi_0 - \cos n\varphi)] \mathbf{L} + \exp[i(m\varphi + \varphi_0 + \cos n\varphi)] \mathbf{R} \right\} \exp\left(\frac{ikr^2}{2z}\right) \exp\left[-\frac{ikrp \cos(\varphi - \phi)}{z}\right] r dr d\varphi \quad (3)$$

where (ρ, ϕ, z) are the cylindrical coordinates, $k = 2\pi/\lambda$ is the wavenumber and λ is the wavelength. Under the modulation of the cosine-azimuthal variant phase factor $\exp(i\cos n\varphi)$, it is difficult to deduce a closed-form expression to describe the focal field intensity distribution. Nevertheless, we can obtain the focal field intensity distribution by numerically integrating Eq. (3).

Like any other cases, the numerical simulation cannot delineate the focal field intensity distribution with a clear analytic expression. In order to consciously manage the focal field, it is urgent to develop a brief tenet for guiding the management. Recently, several works have reported that the LSF can be used to depict the focal field intensity distribution [18,37]. The LSF can be obtained by the Fourier integral with the method of stationary phase and is defined as [38] $f_x = (1/2\pi)\partial\psi/\partial x$, $f_y = (1/2\pi)\partial\psi/\partial y$, where ψ is the phase distribution of the input field $(E(r, \varphi))$, (f_x, f_y) is the orthogonal coordinates in frequency domain. Here, we adopt the LSF to establish a simple mapping relationship between focal field intensity and the pertinent phase distribution of input field. When the vector AAB is encoded with cosine-azimuthal variant phase, the LSF (f_x, f_y) of LH and RH circular polarization components of field described in Eq. (2) can be easily calculated in accordance with the definition. Here, in order to present a concise form of the LSF, we give the LSF expressions (f_ρ) in polar coordinates as follows

$$\mathbf{L}: \begin{cases} f_\rho = \frac{1}{2\pi r} \left| m + n \left(\sin n\phi \cos \frac{n\pi}{2} + \cos n\phi \sin \frac{n\pi}{2} \right) \right|, \\ \phi = \varphi - \frac{\pi}{2} \end{cases} \quad (4a)$$

$$\mathbf{R}: \begin{cases} f_\rho = \frac{1}{2\pi r} \left| m - n \left(\sin n\phi \cos \frac{n\pi}{2} - \cos n\phi \sin \frac{n\pi}{2} \right) \right|, \\ \phi = \varphi + \frac{\pi}{2} \end{cases} \quad (4b)$$

For intuitively presenting the relationship between the LSF distribution of the two spin components and the phases carried by them, it needs to take the parity of phase parameter n into consideration. First, for an odd number of n , i.e., $n = 2k + 1$, k is an integer, Eqs. (4a) and (4b) can be written as

$$\mathbf{L}: f_\rho = \frac{1}{2\pi r} \left| m + n(-1)^k \cos n\phi \right|, \quad (5a)$$

$$\mathbf{R}: f_\rho = \frac{1}{2\pi r} \left| m + n(-1)^k \cos n\phi \right|. \quad (5b)$$

Clearly, the LSF distributions of LH and RH circular polarization components share the identical closed-form expression, which leads to the LSF distributions of the two spin components exhibiting the same profile.

Next, when $n = 2k$, Eqs. (4a) and (4b) evolve into

$$\mathbf{L}: f_{\rho} = \frac{1}{2\pi r} \left| m + n(-1)^k \cos n\phi \right|, \quad (6a)$$

$$\mathbf{R}: f_{\rho} = \frac{1}{2\pi r} \left| m + n(-1)^{k+1} \sin n\phi \right|. \quad (6b)$$

Due to the complementarity of *trigonometric* functions, it is clear that the LSF distributions of LH and RH circular polarization components are spaced from each other along azimuthal coordinates for an even number of n . Based on this, we can make the LH and RH circular polarization components separate from each other along azimuthal coordinates, which indicates the azimuthal spin-dependent splitting.

As for the influence of polarization order m on the LSF distribution, it is quite clear and definite. If $m > n$, there is no null point in frequency domain for LSF. If $m \leq n$, the zero points are determined by the period of the *sinusoidal* or *cosine* function and they intersect at the original point in frequency domain.

Based on the above mentioned discussions, we can consciously design the intensity and polarization distributions of focal field under the guiding of LSF. It should be stressed that, the LSF actually just delineates the geometrical shape of intensity distribution rather than quantify the density of intensity distribution in the focal plane. Under the effect of transverse energy flux arising from the OAM and encoded phase terms, both for the two spin components, the intensity distribution of the two spin components predicted by the identical LSF distribution may be different. According to Eq. (5), due to the ϕ is equal to $\varphi - \pi/2$ and $\varphi + \pi/2$ for the LH and RH circular polarization components, the modulus f_{ρ} of the two spin components begins differently in the azimuthal direction. Besides, the sign of operation is opposite in the modulus f_{ρ} , we can obtain the conclusion that the modulus f_{ρ} increases toward opposite sense along the azimuthal direction. Ultimately, the intensity distributions of the two spin components are symmetric about x axis but may not overlap with each other completely, which results in a spin-dependent splitting along y axes.

3. Simulation results

To corroborate the mapping relationship between LSF and the geometrical shape of the focal field intensity distribution, we depicts the focal intensity distribution obtained from Eq. (3) and LSF distribution of two spin components in Fig. 1. Since the polarization order m does not influence on the azimuthal distribution of LSF distribution, as an example, the polarization order of vector AAB beam is selected as $m = 2$ for different phase parameters ($n = 1, 2, 3,$ and 4) with $\varphi_0 = 0$. In our numerical simulation, the radius of the primary ring r_0 and scaling factor ω are selected as $52 \mu\text{m}$ and $5.4 \mu\text{m}$, respectively.

Figure 1 shows the total focal field intensity I_0 , the intensity of LH (I_L) and RH (I_R) circular polarization components, the contour lines of LSF distributions of LH and RH circular polarization components (the dashed curves in the second and third columns of Fig. 1), as well as the corresponding phase distribution illustrated in the insets. Where the azury solid point (M-point) within each contour line denotes the original point of the curve in Cartesian coordinate system. According to the geometric mapping relationship, the M-point of LSF correspondingly map to the centroid of the focal intensity distribution. Clearly, the focal field intensity distributions of constituent beams (I_L and I_R) agree with the delineations of LSF distributions (dashed curves).

When the phase parameter n is odd, such as $n = 1$ or 3 , the LSF distributions of the two spin components have identical spatial distribution. As pointed out at the end of **Section 2**, the transverse energy flux also has influence on the density of intensity distribution in the focal plane. For instance, when $n = 1$, due to the fact that the two spin components have

opposite transverse energy flux (for more details about the energy flow in the focal field of vector beam, see ref [23].), the intensity distribution along the LSF profile is non-uniform. Although I_R and I_L distributions are symmetrical about x axes, they would not overlap with each other completely. This results in a spin-dependent splitting along y axes. However, when $n = 3$, the LSF distributions present three-fold rotational symmetry, which are similar to three-leaved rose curves. Correspondingly, the intensity distributions (I_0 , I_L , I_R) are like clover. Although the two spin components still move toward opposite sense along the azimuthal direction starting from $\varphi = 0$, it covers three periods in a circle from $\varphi = 0$ to $\varphi = 2\pi$ instead of one period for $n = 1$. This guarantees that the two spin components ultimately coincide with each other and no spin-dependent splitting occurs. Further, we can find that, the peripheral intensity distributions of two spin components are opposite along the azimuthal coordinate, it is an intuitive display of the opposite transverse energy flux [23].

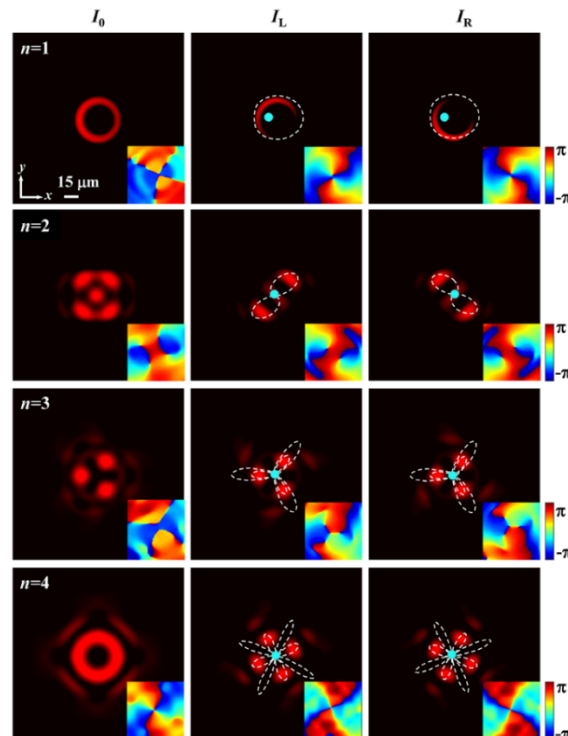


Fig. 1. Simulation intensity distributions of vector AAB with polarization order $m = 2$ and different phase parameters n in the focal plane. The first column denotes the total intensity (I_0); the second and third columns denotes the intensity of LH (I_L) and RH (I_R) circular polarization components. The insets represent the phase profiles. The dashed curves in second and third columns denote the LSF distributions.

When the phase parameter n is even, such as $n = 2$ or 4 , the LSF distributions of the two spin components separate from each other along the azimuthal coordinate. To quantitatively describe the splitting distance of the spin components, we define a parameter Φ to denoting the angular separation of the adjacent two spin components along the azimuthal direction. In the case of $n = 2$, the LSF distributions are like Bernoulli's lemniscate, one is along diagonal direction and the other is along the anti-diagonal direction. That is to say, they are spaced along the azimuthal coordinate and the total intensity ($I_0 = I_L + I_R$) distribution of focal filed present a central lobe and four petals around it. In this case, the angular separation $\Phi = \pi/2$. In the case of $n = 4$, the LSF distributions present four-fold rotational symmetry and the LSF of the two spin components are separated from each other along the azimuthal coordinate. It

resembles the four leafed rose, of which the longer regions denote the null intensity areas. Here, the angular separation $\Phi = \pi/4$. Generally, for $n = 2k$, the angular separation of the adjacent two spin components is $\Phi = \pi/n$, which is actually equal to the period of the modulus f_ρ . Thus, when the phase parameter n of the input field is set as an even number, an azimuthal spin-dependent splitting can be realized. Eventually, the total intensity distribution of focal field forms a full circle. Interestingly, the phase of the total focal field when $n = 4$ has a typically spiral structure, which is similar to a second-order vortex beam.

By means of the mapping relationship between LSF and geometrical shape of the focal field intensity distribution, we can consciously control the spin-dependent splitting and phase distributions of vector AAB by changing the phase parameter n of the encoded cosine-azimuthal variant phase. By employing spatial light modulator, it is easy to imprint desired phase distributions with computer generated hologram (CGH) onto the input field.

4. Experiment results and discussions

Figure 2 illustrates the sketch of the experimental setup. A linearly polarized He-Ne laser ($\lambda = 632.8$ nm) beam is spatially filtered and collimated by the combination of microscopic objective (MO₁) and lens (L₁). The polarization direction of the collimated beam can be rotated by the half-wave plate ($\lambda/2$). Then, the beam is divided by a beam splitter BS₁ into two parts. The reflected one is orderly reflected by the reflection mirrors M₁, M₂, M₃ and BS₂, which is set as a reference beam to interfere with the modulated input beam for retrieving the phase distribution of the focal field. The transmitted one is modulated by the phase spatial light modulator (PSLM) (Holoeye LETO) and polarization conversion system (PCS) to generate the desired input field. The microscopic objective MO₂ is used to magnify the focal field. For the generation of the vector AAB with cosine-azimuthal variant phase described by Eq. (1), the CGH encoded on the PSLM is shown in Fig. 2(a) with intensity distribution written as $t(x,y) = |E_0(r)\exp(i\cos n\varphi) + \exp(ifx)|^2$, where f is the spatial frequency of the CGH. After reflected from the PSLM, the desired beam (shown in Fig. 2(b)) is then spatially filtered by a filter (F) in the first diffraction order of a $4f$ imaging system (consisting of lens L₂ and L₃). Next, the generated AAB is relayed to the PCS to realize the polarization conversion, where a liquid-crystal polarization converter (q -plate) with order $q = 2$ (Thorlabs, WPV10-633) is placed at the image plane of the PSLM as the PCS to generate vector AAB with polarization order $m = 2$.

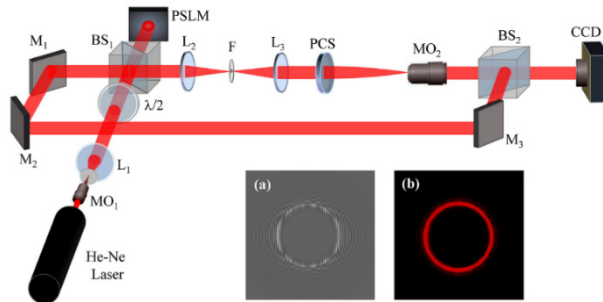


Fig. 2. Schematic of experimental setup. MO: microscopic object; L: lens; $\lambda/2$: half-wave plate; BS: beam splitter; PSLM: phase spatial light modulator; F: filter; PCS: polarization conversion system; M: mirrors; CCD: charge coupled device. The insets: (a) CGH and (b) corresponding intensity distribution behind lens L₃.

Figure 3(a) shows the simulated intensity distribution according to Eq. (1) of a vector AAB with polarization order $m = 2$ and phase parameter $n = 1$. Experimentally, we record the generating vector AAB by a CCD camera closely behind the PCS. Figure 3(b) displays the intensity distribution without a polarization analyzer. To analyze the polarization state of the generated field, we rotate the polarization analyzer with the transmission axis at 0° , 45° , 90° ,

135° angles with respect to the horizontal direction. The corresponding intensity distributions behind the polarization analyzer are depicted in Figs. 3(c)-3(f). The results are in good agreement with the theoretical analysis as indicated by the green double-headed arrows in Fig. 3(a). It should be pointed out that the phase parameter n does not influence on the polarization

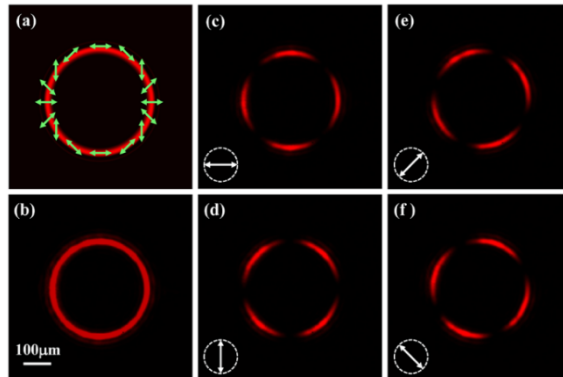


Fig. 3. (a) Simulated and (b) experimentally measured intensity distributions of the vector AAB with polarization order $m = 2$ and phase parameter $n = 1$. (c)-(f) experiment results of the generated vector AAB after passing through a polarization analyzer with the transmission axis denoted by white double-headed arrows within a dashed circle.

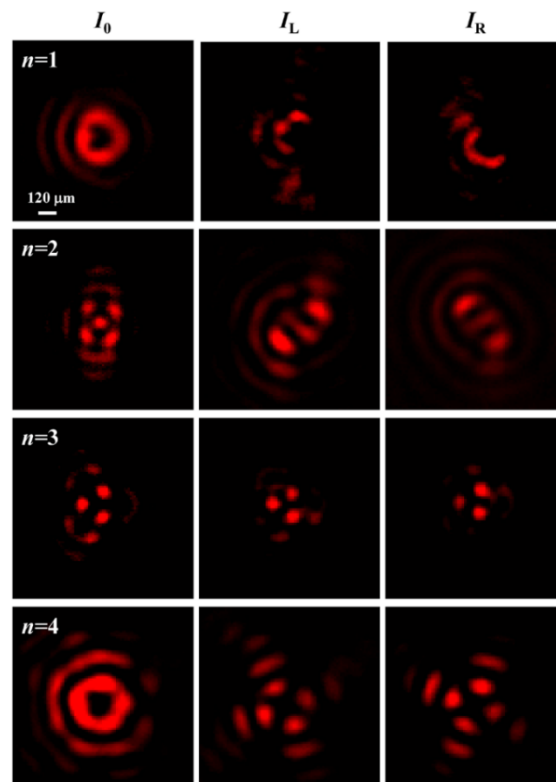


Fig. 4. Experimentally measured intensity distributions of vector AAB with polarization order $m = 2$ and different phase parameters n at the focal plane. The first column denotes the total intensity (I_0); the second and third columns denotes the intensity of LH (I_L) and RH (I_R) circular polarization components.

distribution of the input field, that is to say, when $n = 0, 2, 3$, and 4 , the input intensity distributions without or with the polarization analyzer is the same as the case of $n = 1$.

Figure 4 shows the experimentally measured intensity distribution of total focal field and the two spin components, in the focal plane, when the input field is encoded with different phases. The intensity distribution of LH and RH circular polarization components are measured by the combination of a quarter wave plate, a polarizer and a CCD camera. The experimental results agree with the simulated results shown in Fig. 1. It should be pointed out that the non-uniformity of the intensity distribution of the two spin components is caused by the inhomogeneous transmittance of quarter wave plate due to the manufacturing error.

It is well known that the distributions of Stokes parameter S_3/S_0 (s_3) can be used to depict the circular polarization degree [39]. Hence, we employ the s_3 to denoting the spin-dependent splitting in the focal field of vector AAB. As usual, the s_3 can also be measured by using a typical setup consisting of a quarter wave plate, a polarizer and a CCD camera. In the next, the polarization and phase distribution characteristics of the focal field are analyzed.

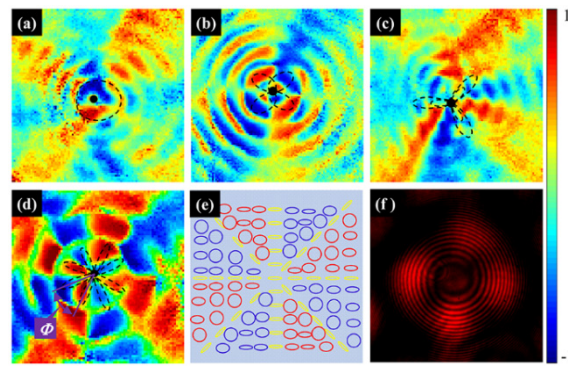


Fig. 5. Distributions of Stokes parameter s_3 of the vector AAB with polarization order $m = 2$ and phase parameters (a) $n = 1$, (b) $n = 2$, (c) $n = 3$, (d) $n = 4$ at the focal plane. The insets depict the corresponding intensity distributions. (e) Theoretical polarization state distribution arising at the focal plane of vector AAB with phase parameter $n = 4$, the red and blue ellipses corresponding to RH and LH circular polarizations, respectively. (f) Interference pattern between a spherical wave and the focal field of the vector AAB with phase parameter $n = 4$. The dashed black curves denote the LSF distributions. Φ denotes the angular separation of the adjacent two spin components.

To verify the spin-dependent splitting predicted by the LSF distribution, we give the LSF distribution (dashed black curves) and s_3 of the focal field as follows. Experimentally, the measured angular separation Φ is equal to the angle between the two lines starting from the center and passing respectively through the maximum of the intensity for one of the two components as illustrated in Fig. 5(d). In Fig. 5(a), for $n = 1$, the focal field presents a giant spin splitting which is similar to photonic spin Hall effect of fan-shaped cylindrical vector beam occurring at the focus [36]. As stated in the previous section, the intensity distributions I_R and I_L are symmetrical about x axes, which results in LH and RH circular polarization components splitting along y axes. The angular separation of the adjacent two spin components is about $\Phi = \pi$. In the case of $n = 2$, the center of the focal field is linearly polarized, and two LH circular polarization lobes are focused along the diagonal direction while two RH circular polarization lobes are focused along the anti-diagonal direction as the LSF indicates as shown in Fig. 5(b). The angular separation of the adjacent two spin components is about $\Phi = \pi/2$. The total intensity pattern presents a center lobe surrounded by four side lobes, which align along the LSF distributions of the two spin components. In the case of $n = 3$, the total focal field intensity distribution presents three main lobes which are all linearly polarized. It demonstrates the theoretic prediction that the spin-dependent splitting does not occur. Note that, three spin pairs are around the three main lobes as shown in Fig.

5(c), which denotes the peripheral intensity of the two spin components. In the case of $n = 4$, as indicated by the LSF distribution (for better visibility, we leave out longer regions of LSF), the LH and RH circular polarizations are spaced from each other along the azimuthal coordinate and completely compensated resulting in the formation of a full circle. As shown in Fig. 5(d), the s_3 distribution actually presents an azimuthal spin-dependent splitting, which is similar to the focal field polarization distribution where the azimuthally polarized beam modulated by multi-azimuthal masks [26]. In this case, the angular separation of the adjacent two spin components is about $\Phi = \pi/4$. As we can see, except for the experimental imperfections caused by the manufacturing error of the quarter wave plate, the experimentally measured angular spin splitting agrees with the theoretical prediction. Our main interest focuses on the spin-dependent splitting phenomena, the quantitative description of spin splitting presented here is just expected to provide an intuitively impression.

According to the experimentally measured s_3 distribution as shown in Fig. 5(d), the theoretic polarization state distribution is depicted in Fig. 5(e), which presents azimuthal variant polarization states and forms azimuthal SAM gradient. It should be stressed that this azimuthal SAM gradient cannot trigger the occurrence of OAM. As has been demonstrated in [28,40], only the radially variant vector field and SAM gradient can generate OAM without spiral phase. However, as the prediction of the theory analysis, for second order ($m = 2$) vector AAB with $n = 4$, the phase of the focal field forms a spiral structure, which is similar to the second-order vortex beam. In order to confirm this spiral phase structure, we experimentally introduce another reference beam to interfere with the focal field. Since the focal field is too small to be directly observed in our implementation, we introduce a microscopic objective MO₂ to magnify the focal field as shown in Fig. 2. The magnified focal field and the reference beam are combined by the beam splitter BS₂ to interfere. The interference pattern is recorded by the CCD camera. As shown in Fig. 5(f), the spiral fringe demonstrates that the focal field has a spiral phase with topologic charge $l = 2$, which suggests the existence of OAM. Here, the formation of spiral phase originates from the influence of the encoded cosine-azimuthal phase through the abruptly autofocusing process.

Note that, according to the LSF distribution, for larger even numbers, e.g., $n = 6, 8, 10 \dots$, the total intensity distributions of focal fields also form a complete circle just like that of $n = 4$, and the s_3 distributions also indicate azimuthal spin splitting. Nevertheless, their focal field do not carry spiral phase. Namely, the focal field has a spiral phase only when the phase parameter n and polarization order m satisfy the relationship of $n = 2m$, and then the topologic charge of the spiral phase equals to the polarization order m .

5. Conclusions

In conclusion, the spin-dependent splitting of vector AAB was realized by encoding cosine-azimuthal variant phases. Based on the LSF of the two spin components, an approximation mapping relationship between the focal field intensity and the phase profile of the input field is established. By modulating the cosine-azimuthal variant phase parameter n , the spin-dependent splitting and OAM in the focal field can be consciously managed. Such optically mediated intensity, polarization and OAM distributions could be significant useful in focal engineering for special functionality. These results can provide new insights in controlling the spin-orbit coupling and optical micro manipulation.

Funding

973 Program (2012CB921900); National Natural Science Foundations of China (NSFC) (11404262, 11634010, 61675168, U1630125 and 61377035); Fundamental Research Funds for the Central Universities (3102014JCQ01084, and 3102015ZY057); the Natural Science Basic Research Plan in Shaanxi Province (2015JQ1026); and the Innovation Foundation for Doctor Dissertation of Northwestern Polytechnical University (CX201629).